

Article

# Calculation and Characterization of Air Void in Mortar of the Hot Mix Asphalt (HMA) Based on CT Scanning and Image Analysis Methods

Li-Heng Shu <sup>1</sup>, Fu-Jian Ni <sup>1,\*</sup>, Ji-Wang Jiang <sup>1,\*</sup>, Zi-Li Zhao <sup>1</sup> and Zhao-Yuan Guo <sup>1,2</sup><sup>1</sup> School of Transportation, Southeast University, Nanjing 211189, China<sup>2</sup> Jiangsu Provincial Transportation Engineering Construction Bureau, Jiangsu Transportation Building, No. 69 Shigu Road, Nanjing 210004, China

\* Correspondence: nifujian@gmail.com (F.-J.N.); jiang\_jiawang@seu.edu.cn (J.-W.J.)

**Featured Application:** Authors are encouraged to provide a concise description of the specific application or a potential application of the work. This section is not mandatory.

**Abstract:** The air void content is one of the most important volumetric properties of asphalt matrixes, such as asphalt mixtures or mortars, because it can greatly affect the performance of the matrix. At the mixture level, there are standardized methods for measuring the air void content, which is an important design parameter of a mixture. However, at the mortar scale, no unified method has been proposed to determine the air void content corresponding to the asphalt mixture. Therefore, this research aims to, first, characterize the air void distribution within the mortar of an asphalt mixture and then develop an updated theoretical method for calculating the air void content of asphalt mortar. The internal structures of air voids from three commonly used asphalt mixtures with different gradations were captured using an industrial CT scanning technique and then morphologically characterized using the image analysis method. Three-dimensional models of the air voids were reconstructed, and the air void content calculated from the CT images was also verified by density tests. The scanning results show that the air void content and air void size fit the cumulative Weibull curve. The results show that the nominal maximum particle size (NMPS) of mortar and the mixture air void content were the main parameters that affected the mortar's air voids. The mortar air void content had linear relationships with both the mixture air void content and the mixture asphalt aggregate ratio. The mortar air void content was more sensitive to the NMPS of the asphalt mixture compared with the air void content or asphalt aggregate ratio of the mixture. This research provides a quantitative method to calculate the air void content of asphalt mortar within a mixture, which may help in the matrix design of mortar.

**Keywords:** asphalt mortar; air void calculation; CT scanning; image analysis



**Citation:** Shu, L.-H.; Ni, F.-J.; Jiang, J.-W.; Zhao, Z.-L.; Guo, Z.-Y. Calculation and Characterization of Air Void in Mortar of the Hot Mix Asphalt (HMA) Based on CT Scanning and Image Analysis Methods. *Appl. Sci.* **2023**, *13*, 652. <https://doi.org/10.3390/app13010652>

Academic Editor: Syed Minhaj Saleem Kazmi

Received: 2 November 2022

Revised: 26 December 2022

Accepted: 27 December 2022

Published: 3 January 2023



**Copyright:** © 2023 by the authors. Licensee MDPI, Basel, Switzerland. This article is an open access article distributed under the terms and conditions of the Creative Commons Attribution (CC BY) license (<https://creativecommons.org/licenses/by/4.0/>).

## 1. Introduction

Asphalt mixtures, consisting of aggregate, asphalt and air voids, can be divided into a coarse aggregate phase and an asphalt mortar phase. Coarse aggregates comprise the skeleton and occupy most of the volume, while asphalt mortar fills in the intervals of the coarse aggregates and works as a bonding material between the coarse aggregates [1,2]. The air voids in an asphalt mixture can be distinguished as open or closed porosities, and many studies have focused on the size and distribution of the voids in a mixture and their influence on the pavement performance [3]. The air void content is a vital parameter which characterizes an asphalt mixture, and it is measured by one minus the ratio of the bulk density to the maximum theoretical density [4,5]. To obtain a stable mixture, control parameters are used, such as the passing rate, asphalt aggregate ratio and air void content. Among these constituents, the air void content has a significant effect on pavement

performance [6]. The air void content is controlled by design, and the compaction has a direct impact on multiple mixture's performance, such as the fracture resistance [7–9], high-temperature creep resistance [10] and fatigue performance [11]. For example, a mixture with a larger air void content would be less stiff and have a smaller modulus compared with those with a smaller air void content, while a mixture with a certain air void percent has the best anti-rutting performance [12]. The aging rate of service pavement mixtures is also affected by the air void content [13–15]. Thus, the air void content is another vital control parameter for compaction, since dense and loose compactions in the same type of mixture have different volume properties and pavement performances [16].

The multiscale approach to asphalt mixtures has drawn increasing attention at the multiscale level, such as mortar and mastic, when comparing the asphalt materials' performance at this scale. Mortar, or FAM (fine aggregate matrix), is the transition scale between asphalt binder and asphalt mixture, which has both the viscoelastic properties of asphalt binder and dynamic modulus and fatigue performance similar to asphalt mixture [16]. With these features, mortar research on asphalt mixtures has been vital for understanding mixture performances or distress mechanisms [17]. With the numerous studies on mixtures, increasing attention has been paid to the mortar phase in a mixture [18]. Currently, as there is no standard specification for mortar preparation, testing and evaluation, many attempts have been made to reveal the manufacturing method, various performances and relationships of binder and the mixture of a mortar [18]. For further research on mortar, when manufacturing it in laboratories, it should have similar physical properties as pavement. However, the actual void percent and distribution condition of mortar in mixtures have still not been fully revealed. Researchers have studied void size and distribution in mortar and have made much progress, but the calculating the accurate air void content of mortar is still unclear. For example, in [19], less than 25% of the air void content for a 1.18 mm mortar and approximately 50–75% of the air void content in a NMPS 2.36 mm mortar were reported [19,20], but a more direct and accurate solution is needed.

The measurement of the air void content in mixtures has been well developed. The conventional method calculates the ratio of the volume of the air void content in the mixture to that of the whole mixture containing both solids and air voids [21]. With high-tech approaches, such as computerized tomography (CT) [22,23], air void details, such as their size and distribution in an asphalt mixture, can be characterized and analyzed. CT is a meso-structure testing approach that provides details on voids inside of samples to determine and evaluate the size and number of voids [24]. CT images with high-energy X-ray scanning of the sample can be used to illustrate an image array. Asphalt has a lower reflection rate, and painted as dark areas and aggregates have a larger reflection rate than painted as light areas. DIP is a quantitative approach that can illustrate the different phases in scanned images [10]. Using the DIP threshold segmentation method, such as the Otsu and modified Otsu method, with erosion and dilation [25], the asphalt, aggregate and air void parts can be separated and quantized. Then, the image information of a mixture or mortar slice can be acquired for mixture interstructure evaluation, such as contact indices, asphalt mortar thickness, aggregate particle orientation and air void distribution indices. CT and DIP [26] used together are a popular approach to researching the accurate interstructure of asphalt mixtures and asphalt mortars [24]. This approach is widely applied in evaluating mixture and pavement meso-structures through load and failure procedures, aging and recycling procedures and complete and distress procedures. Air void content is characterized using a coded program or commercial software. In addition to mixture samples, characterization of the mortar's interstructure can also be studied using this approach.

## 2. Objective

The objective of this study was to calculate the mortar air void content based on CT scanned samples' volume information and then to calculate the mortar's volumetric properties. Although researchers can assume the mortar's volumetric properties, which makes

manufacturing easier, mortar material with similar volumetric properties as a mortar mixture would be useful when studying interstructure stress and volume change. Scholars have conducted similar studies testing the performance of asphalt mortar and coarse aggregate asphalt separately and then deciding on the optimal gradation composition of the mortar and coarse aggregate asphalt for the design of a mixture [27]. The challenge of mortar theorization and application is that there is no clear definition of the volumetric properties of mortar. When discussing the air void percent, it means the void percent of a mixture. The void percentage in a mortar and in the coarse aggregate will not affect the mixture’s air void value, but they may have different mortar air void contents. There are two existing methods to conduct mortar research. Firstly, assuming that the air voids that exist in mortar are similar to those in a mixture, the mortar design is conducted the same as for mixture design. The usage of each part and the volumetric properties can be controlled. Secondly, when studying the quantitative air void properties in mortar through CT, the results are accurate but disposable, which means that the mortar’s air void content and the mortar’s air void percent in the mixture can only be obtained at high cost. Therefore, this study attempted to combine the accuracy of the CT approach and the certainty of the mixture design approach to develop a general and relatively accurate approach to mortar air void determination.

To achieve this objective, three types of asphalt mixtures with different nominal maximum particle size (NMPS) were manufactured in the laboratory and scanned using an industrial CT scanner. The scanned images were processed with binarization and threshold segmentation. Then, all of the voids in mixture were identified, numbered, counted and fitted with a statistical curve. The small voids were counted in the mortar, while the large ones were counted in the mixture; then, the identified air voids in the mortar of the mixture could be calculated. In addition, a new method to calculate the mortar air void content was designed and promoted based on the specific surface area method. There were mortars with different NMPS for each mixture; thus, in total, there were 12 types of mortar air voids calculated, and the sensitivity of the mortar air void content to the mixture’s air void content and asphalt aggregate ratio was analyzed.

### 3. Materials Preparation

#### 3.1. Commonly Used Mixture Designs

Basalt and limestone are the most widely used asphalt mixture aggregates in Jiangsu Province. The surface layer uses basalt, while the middle and bottom layers use limestone. Three types of dense mixtures with various nominal maximum particle size (NPMS), AC-13, AC-20 and AC-25, were designed in the laboratory, and their gradation and design are common in Jiangsu. Basalt was used in AC-13 as the surface layer, and limestone was used in AC-20 and AC-25 for the middle and bottom layers. The mixture gradation and design are shown below. Then, these mixtures were mixed and compacted by a Marshall compactor for 75 cycles. All of the design symbols and abbreviations of the mixture design correspond to asphalt pavement construction standards in China [28]. All of the design results are the same as commonly used pavement asphalt of Jiangsu expressways. The designed air void content for AC-13, AC-20 and AC-25 were 4.0%, 4.5% and 5%. The designed asphalt aggregate values for AC-13, AC-20 and AC-25 were 5.0%, 4.5% and 4.2%. The asphalt mixture gradation passing rates are shown in Table 1. The surface layer of AC-13 was finer, so it had a larger passing rate (13.2 mm) and fine aggregate (<4.75 mm) particles. The bottom layer of AC-25 had a smaller fine aggregate passing rate.

**Table 1.** Commonly used mixture designs.

Passing Rate %	31	26.5	19	16	13	9	4.75	2.36	1.18	0.6	0.3	0.15	0.075
Gradation	100	100	SBS PG76-22 AC-13 5% asphalt aggregate ratio 4% air void content										
Gradation	100	100	100	100	94.9	67.0	38.4	33.1	26.0	17.0	12.0	9.3	5.9
Gradation	100	100	SBS PG76-22 AC-20 4.5% asphalt aggregate ratio 4.5% air void content										
Gradation	100	100	97.1	87.0	76.0	59.6	43.8	27.7	21.6	14.3	8.8	7.1	5.7
Gradation	100	100	AH 70# AC-25 4.2% asphalt aggregate ratio 5% air void content										
Gradation	100	100	96.1	83.2	73.1	60.2	41.1	29.6	23.3	15.6	9.9	8.1	6.6

### 3.2. Mortar Design

To obtain general results, maximum aggregate sizes from 0.6 to 4.75 mm (0.6, 1.18, 2.36 and 4.75 mm) were used for the mortar design. These sizes are the same as the sieve size used for asphalt mixtures on China’s mainland. The asphalt aggregate ratio of the mortar was calculated by the specific surface area method, and the mortar design results are shown in Figure 1, and the gradation of each mortar is shown in Table 2, which also shows the aggregate sieving results of the mortar.

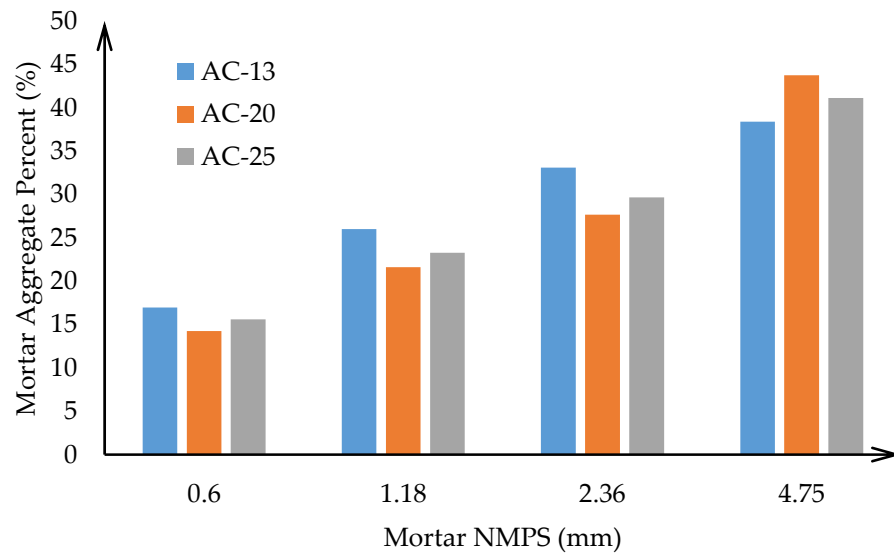


Figure 1. Asphalt aggregate ratio.

Table 2. Mortar design results.

Mortar Type Sieve Size (mm)	Passing Rate (%)							Asphalt Aggregate Ratio (%)
	4.75	2.36	1.18	0.6	0.3	0.15	0.075	
AC-13								
0.6 Mortar				100.0	70.5	54.6	34.6	20.16
1.18 Mortar			100.0	65.3	46.0	35.7	22.6	14.85
2.36 Mortar		100.0	78.6	51.3	36.2	28.0	17.8	12.82
4.75 Mortar	100.0	86.2	67.7	44.2	31.2	24.2	15.3	11.69
AC-20								
0.6 Mortar				100.0	61.6	50.0	40.2	21.39
1.18 Mortar			100.0	66.0	40.6	33.0	26.6	15.87
2.36 Mortar		100.0	78.0	51.5	31.7	25.7	20.7	13.57
4.75 Mortar	100.0	63.3	49.4	32.6	20.1	16.3	13.1	9.06
AC-25								
0.6 Mortar				100.0	63.3	52.1	42.3	18.72
1.18 Mortar			100.0	67.0	42.4	34.9	28.4	14.04
2.36 Mortar		100.0	78.5	52.6	33.3	27.4	22.3	12.02
4.75 Mortar	100.0	72.1	56.6	37.9	24.0	19.8	16.0	9.12

The design of the aggregate rate of the mortar was calculated using Equations (1)–(3).

$$SA_r = \sum(P_i \times FA_i) \tag{1}$$

where  $SA_r$  is the total surface area of the mortar ( $m^2/kg$ );  $P_i$  is the passing rate of each mortar particle aggregate (%);  $FA_i$  is the specific surface area of the particle size aggregate; and  $r$  ( $0 < r < \text{mixture NMPS}$ ) is the NMPS of the calculated mortar (mm).

$$P_{a-r} = \frac{(SA_r/SA) \times P_a}{P_r} \times 100 \quad (2)$$

where  $P_{a-r}$  is the asphalt aggregate ratio of the mortar (%);  $SA$  is the total surface area of the selected mixture ( $m^2/kg$ );  $P_a$  is the asphalt content of the selected mixture (%); and  $P_r$  is the mortar mass rate of the mixture (%).

$$P_{si-r} = 100 - \frac{P_{a-r}}{100 + P_{a-r}} \quad (3)$$

where  $P_{si-r}$  is the aggregate rate of the mortar (%).

Equations (2) and (3) determine the usage of asphalt in designing the mortar.  $SA$  is the total surface area of all aggregates. This step in the mortar design can be conducted using the specific surface area method. Assuming that all of the aggregate particles had the same asphalt film thickness, the specific surface area method was used for deciding the mortar asphalt dosage.

#### 4. CT Scan and Image Processing

##### 4.1. CT Scan Test

CT scanning is an accurate and commonly used method for confirming the internal structure of asphalt samples. The investigation of the air void distribution characteristics of the laboratory fabricated samples was conducted with CT scanning tests on the three types of asphalt mixture. The AC-13, AC-20 and AC-25 samples were compacted in the laboratory. Then, a high-resolution industrial CT scanner, Compact-255 by YXLON, was used for scanning. The volumetric properties of the samples are presented after the introduction of the CT scanners, as well as the number and distribution of the air voids of the mortar in asphalt mixtures.

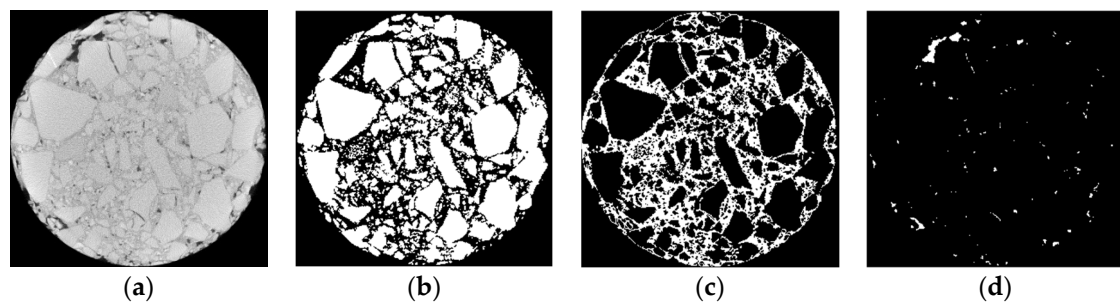
To obtain the same mixture used in Jiangsu, the CT scanned samples' diameter was 101 mm and the height was 63.5 mm. The mixture samples were compacted by a Marshall striker to the designed air void content in the laboratory. Figure 2 shows a picture of the three mixture samples. In the scanned images, the light areas are the stone, while the black areas are voids, whether air voids or outside. The scanned images had a resolution of  $0.11 \text{ mm} \times 0.11 \text{ mm}$ . The distance between neighboring images was 0.11 mm. The scanned images are grayscale map with 256 bit depth. The voxels of the voids in the CT images correspond to the volume in the slices of the scanned sample; each fraction was identified and marked. The 2D images were analyzed using the MATLAB program.



Figure 2. Samples of three mixture types.

#### 4.2. Image Processing

Each sample's images were used without the top and bottom 10 mm to obtain stable void data. The scanned images consisted of voxels (volume elements) with different gray scales. The resolution of the images was  $0.11 \text{ mm} \times 0.11 \text{ mm}$ , and the distance between adjacent images was 0.11 mm. Image enhancement was the first step for the scanned images to make unclear details clearer and to reduce uninteresting regions. CT scanning of the sliced images was conducted, and median filter and grey level transformation were used [29]. The second step was image segmentation, which was based on ring region and Otsu method [30]. The circle image was cut into 6 different rings to reduce the brightness change in the radial direction, and the Otsu method was used for each ring for the segmentation and then combined back into one picture [31]. For example, the image segmentation results for AC-20 is shown in Figure 3; from left to right is the scanned image, voids, mortar and aggregate, which are plotted in white at the same position as in the scanned image.



**Figure 3.** Otsu segmentation of AC-20: (a) scanned; (b) coarse aggregate; (c) mortar; (d) air voids.

Then, post-processing was applied, and the particle diameters and void diameters were calculated by assuming that all of the particles in the picture were circles [24,29,32]. After a 2D void analysis, the 2D slice images were integrated and 3D models were constructed using industrial CT software; the different materials were identified as coarse aggregate, mortar and voids. In this section, mortar with NMPS 2.36 mm and no air voids was used, since this NMPS is widely selected. Then, the voids were classified by volume and characterized using Equations (4) and (5).

The 2D equivalent diameters of the particles were as in Equation (4):

$$\text{Feremeter2} = 2\sqrt{\text{Area}/\pi} \quad (4)$$

where Feretmeter2 is the equivalent diameter (mm), and Area ( $\text{mm}^2$ ) is the area of the voids in the image.

The 3D equivalent diameters of the particles were as in Equation (5):

$$\text{Feremeter3} = 2\sqrt[3]{(3 \times \text{Volume})/(4 \times \pi)} \quad (5)$$

where Feretmeter3 is the equivalent diameter (mm), and Volume ( $\text{mm}^3$ ) is the area of the voids in the image.

## 5. Void Analysis and Mortar Void Percent

### 5.1. 2D Void Analysis

The multiscale approach to asphalt pavement often divides the asphalt mixture into coarse aggregate, mortar and voids [33,34]. All voids are counted when designing a mixture, but for mortar, some voids are too large. In this study, a simple but effect method is introduced where only the voids smaller than the NMPS are counted as voids in mortar, while voids lager than the NMPS are counted as voids not in the mortar but in the mixture.

An analysis of the 3D model followed the same rule [18]. The voids in the mortar example are shown in Figure 4.

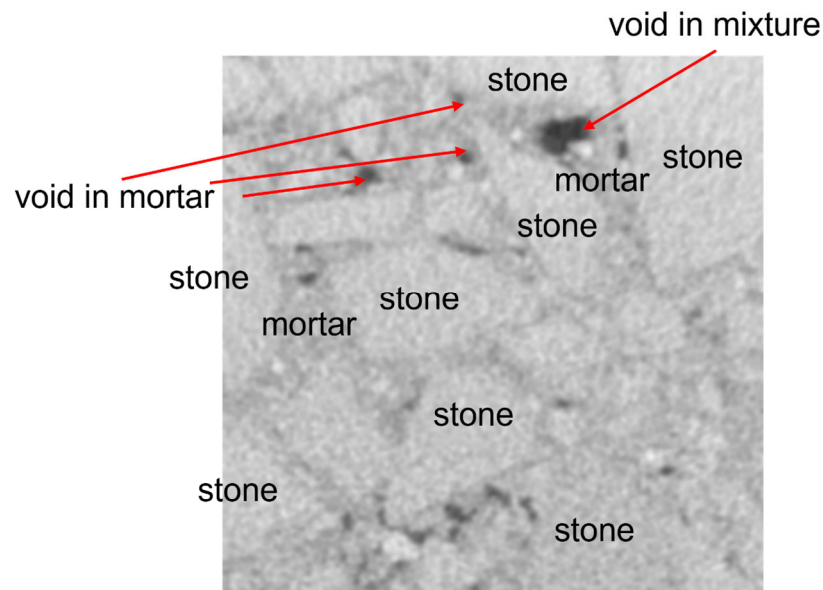


Figure 4. Mortar with voids.

With image processing, each void’s details were identified. By conducting the void static using the equivalent diameter, as in Equation (4), the void passing rate at an integer void size was identified. The void passing rates are introduced and shown in Table 3, and the void passing rate can be regarded as the concept of “void gradation”, which is similar to the mixture aggregate gradation.

Table 3. Void passing rate with different void sizes of the different mixtures.

Mixture Type	Void Passing Rate (%)					
	1 mm	2 mm	3 mm	4 mm	5 mm	6 mm
AC-13	13.2	38.6	63.4	81.4	91.8	96.9
AC-20	10.8	32.1	54.8	73.2	85.8	93.2
AC-25	10.9	28.5	46.6	62.4	74.9	84.0

Void gradation is defined as the passing rate of the void size, similar to the aggregate gradation, and the calculation of the void gradation of the mixture and the results are as follows: Using Table 3, we can obtain the void percent in mortar using Equation (6). The cumulative void percent followed the cumulative Weibull distribution. The cumulative value and regression value of the void gradation of the three mixtures are shown in Figure 5. With the fitting curve, the void percent of any size can be calculated. For mortar with the maximum particle of 2 mm, the AC-13 mortar had 38.6% voids for the total void content of 4.1% in the mixture, while AC-20 had 32.1% of 4.2% and AC-25 had 28.5% of 4.4%. For the mortar with the maximum particle of 4 mm, the AC-13 mortar had 81.4% of the total void content for 4.1% of the mixture, while AC-20 had 73.2% for 4.2% and AC-25 had 62.4% for 4.4%. The cumulative Weibull curve was fitted with the void passing rate and obtained relatively ideal fitting results. With this we could obtain the void percent of the mortar with a common NPMS. The regression of the cumulative Weibull curve of the three mixture’s air void sizes is shown in Figure 5, and the void percent results of the commonly used sizes are shown in Figure 6. The parameter  $v_r$  is the void percent (%) which is the percent of air voids that exist in certain types of mortar [29].

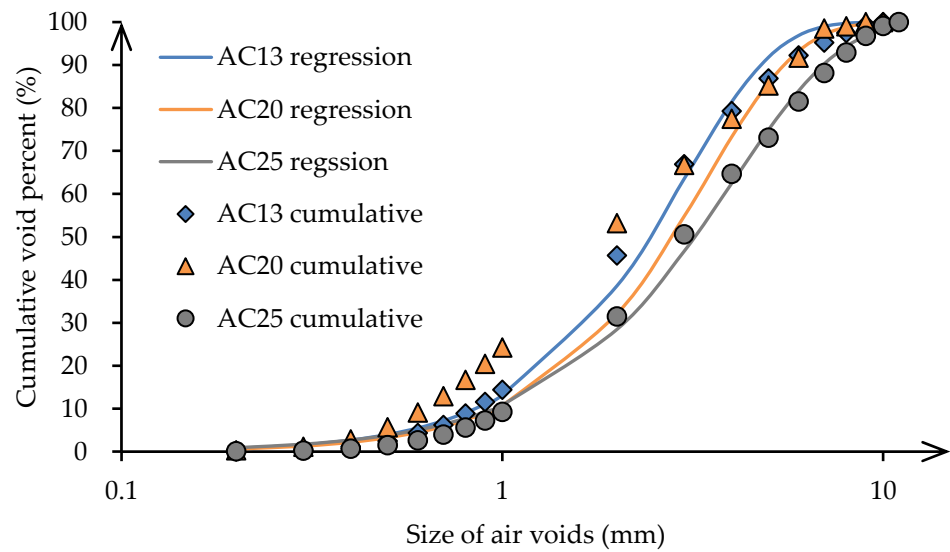


Figure 5. Air void cumulative and regression values of the cumulative Weibull curve for the three mixtures.

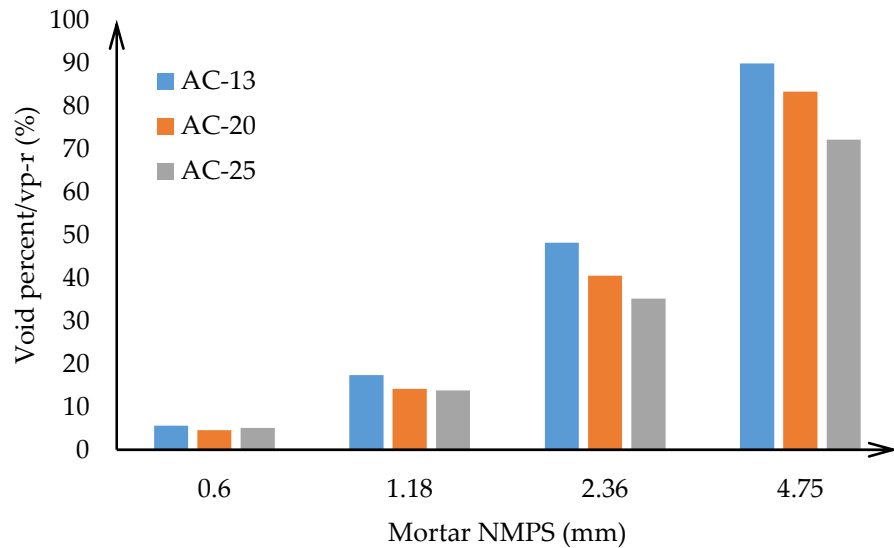


Figure 6. Mortar void percent for the mortar in the mixture.

The void passing rate of a mixture fitting the cumulative Weibull curve is calculated using Equation (6):

$$F(x) = [1 - e^{-(x/\lambda)^k}] \times 100, x \geq 0 \tag{6}$$

where  $x$  is the void size (mm);  $\lambda$  (mm) and  $k$  (dimensionless) are the shape parameters; and  $F(x)$  is the fitted passing rate responding to size  $x$  (%). The parameter  $\lambda$  controls the void size distribution, and the larger the value of  $\lambda$ , the larger the scale of the air void size. Parameter  $k$  controls the void size concentration, and the larger the value of  $k$ , the greater the concentration of air voids at the middle size.

Figure 5 displays the cumulative Weibull curve and fitting curve of the three mixtures. Using these curves, the cumulative void percent can be obtained. For a 0.6 mm mortar, the mortar void percent is 5.1% to 5.5% of the total mixture air void content of 4.1% to 4.4%; for a 1.18 mm mortar, this value is 13.8% to 17.4% of 4.1% to 4.4%; for a 2.36 mm mortar, it is 35.1% to 48.1% of 4.1% to 4.4%; and for a 4.75 mm mortar, this value is 72.1% to 89.8% of 4.1% to 4.4%. This also means that most of the void volume is less than 4.75 mm, nearly half of them are less than 2.36 mm and only a slight amount of the void volume is less than

0.6 and 1.18 mm. For a 1.18 mm mortar size, the void percent results are in the range of other studies [20], verifying the reliability of both the previous and this study.

5.2. 3D Void Analysis

The sliced images were reconstructed as a 3D model, and the total voxel number of the coarse aggregate, mortar (without voids) and voids were plotted. A three-dimensional model of AC-13 with voids is shown in Figure 7. The voids, after measuring tests and CT scanning, were compared, and the results are shown in Table 4. In this section, all of the mortar mentioned had an NMPS of 2.36 mm for research consistency and one NMPS mortar was enough to clarify the different parts of the mixture [32]. Then, the air void content of the three laboratory manufactured asphalt mixtures were calculated using Equation (7). The density of the mixture samples was tested by the surface dry method, and the theoretical maximum density was tested by the vacuum method. The two methods follow the “Standard Test Methods of Bitumen and Bituminous Mixtures for Highway Engineering”. Table 5 shows the voxel statistic results of air void, mortar and coarse aggregate. And Table 4 shows that the CT scanned air void content matched the tested air void content.

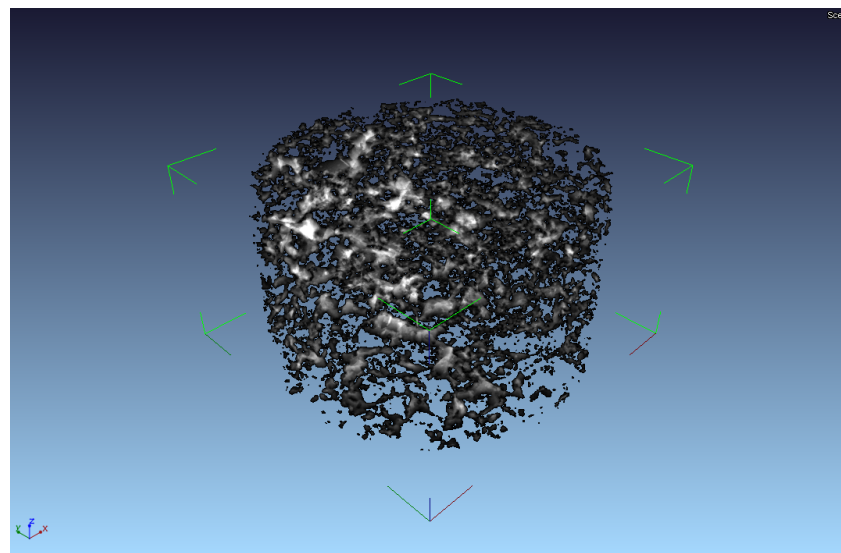


Figure 7. Illustration of the 3D model of the voids for AC-13.

Table 4. Air void content, coarse aggregate volume and deviation of the CT and test results.

Mixture Type	Air Void Content			
	Designed (%)	Tested (%)	Scanned (%)	Deviation (%)
AC-13	4	4.1	4.2	0.1
AC-20	4.2	4.2	4.1	−0.1
AC-25	4.5	4.4	4.6	0.2

Table 5. Calculation results of the air voids, mortar and coarse aggregate volume.

Mixture Type	Air Void		Mortar (without Voids)		Coarse Aggregate	
	Voxel	Volume (mm <sup>3</sup> )	Voxel	Volume (mm <sup>3</sup> )	Voxel	Volume (mm <sup>3</sup> )
AC-13	$1.08 \times 10^7$	15,646.3	$8.97 \times 10^7$	129,641.1	$1.57 \times 10^8$	227,244.5
Percent (%)		4.2		34.8		61
AC-20	$1.58 \times 10^7$	22,842.0	$1.27 \times 10^8$	183,293.0	$2.43 \times 10^8$	350,986.6
Percent (%)		4.1		32.9		63
AC-25	$1.57 \times 10^7$	22,721.8	$9.87 \times 10^7$	142,752.1	$2.27 \times 10^8$	328,478.1
Percent (%)		4.6		28.9		66.5

The aggregates and asphalt parts in the mortar (without void) occupied a larger volume percent in AC-13 than that in AC-20, and the aggregates and asphalt parts in the mortar occupied a larger volume percent in AC-20 than that in AC-25. The coarse aggregate volume percent of AC-13 was less than AC-20, and the coarse aggregate volume percent of AC-20 was less than AC-25. The larger the mixture’s NMPS, the less the mortar, and the larger the mixture’s NMPS, the larger the coarse aggregate percent.

**6. Mortar Air Void Content Calculation Equation**

Based on the preparation work, the method to calculate the designed mortar air void content with various NMPS and different mixture types was introduced. The calculation method consists of several equations from Equations (7)–(13), and the calculation results are shown in Figure 8.

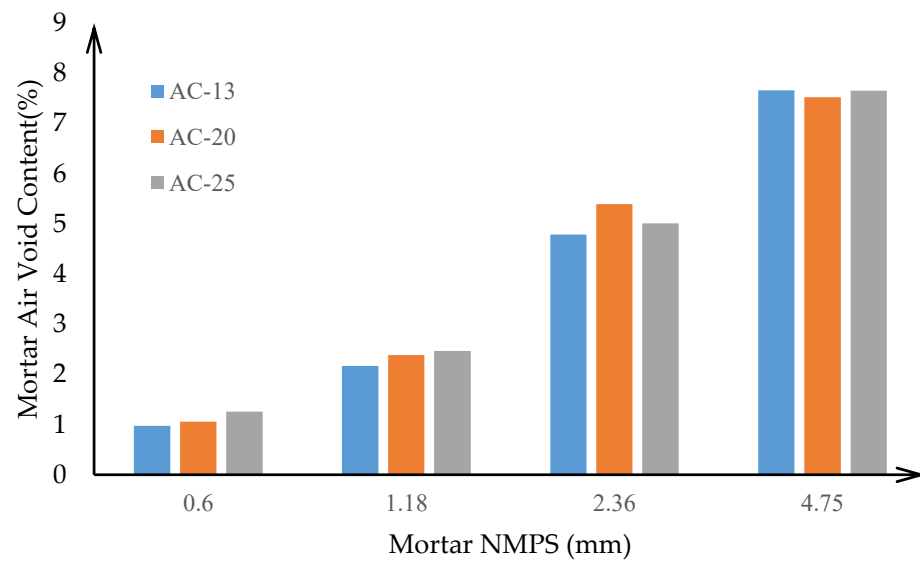


Figure 8. Mortar air void content calculation results.

Equation (7) is the calculation for the mixture air void content:

$$VV = \left( 1 - \frac{\gamma_f}{\gamma_t} \right) \times 100 \tag{7}$$

where  $VV$  is the designed mixture air void content (%);  $\gamma_f$  is the measured sample density ( $\text{g}/\text{cm}^3$ ); and  $\gamma_t$  is the theoretical maximum density ( $\text{g}/\text{cm}^3$ ) of the mixture sample.

The effect density of the mortar is determined by Equation (5), which is similar to the effect density of the mixture aggregate. Equations (8)–(12) determining the effect density for the mortar, which is vital for calculating the mortar voids.

The bulk density,  $\gamma_{sb-r}$  ( $\text{g}/\text{cm}^3$ ), of the mortar aggregate with  $r$  NMPS is calculated as per Equation (8):

$$\gamma_{sb-r} = \frac{100}{\frac{P_{1-r}}{\gamma_{1-r}} + \frac{P_{2-r}}{\gamma_{2-r}} + \dots + \frac{P_{n-r}}{\gamma_{n-r}}} \tag{8}$$

where  $P_{i-r}$  is the mass content of aggregate particle  $i$  (%);  $\gamma_{i-r}$  is the bulk density of mortar particle  $i$  ( $\text{g}/\text{cm}^3$ ),  $1 \leq i \leq n$ .

The apparent density,  $\gamma_{sa-r}$  ( $\text{g}/\text{cm}^3$ ), of the mortar aggregate with  $r$  NMPS is calculated as per Equation (9):

$$\gamma_{sa-r} = \frac{100}{\frac{P_{1-r}}{\gamma'_1} + \frac{P_{2-r}}{\gamma'_2} + \dots + \frac{P_{n-r}}{\gamma'_n}} \tag{9}$$

where  $\gamma'_i$  is the bulk density of mortar particle  $i$  ( $\text{g}/\text{cm}^3$ ),  $1 \leq i \leq n$ .

The effective density,  $\gamma_{se-r}$  ( $\text{g}/\text{cm}^3$ ), of the mortar aggregate with  $r$  NMPS is calculated as per Equation (10):

$$\gamma_{se-r} = C \times \gamma_{sa-r} + (1 - C) \times \gamma_{sb-r} \quad (10)$$

where  $C$  is the aggregate absorption index (%).

The aggregate absorption index,  $C$ , is calculated by Equation (11), which is a widely used empirical equation in China and also recommended in the standard for the use of modified asphalt mixtures. Equation (11) is as follows:

$$C = 0.033W_{x-r}^2 - 0.296W_{x-r} + 0.9339 \quad (11)$$

where  $W_{x-r}$  is the water absorption percent (%).

The water absorption percent,  $W_{x-r}$ , is calculated as per Equation (12):

$$W_{x-r} = \left( \frac{1}{\gamma_{sb-r}} - \frac{1}{\gamma_{sa-r}} \right) \times 100 \quad (12)$$

Finally, the air void content of a given mortar NMPS can be calculated by Equation (13), which clarifies each phase's volume, including the air voids in the mortar, mortar aggregate and asphalt. In this equation,  $v_{p-r}$  is the void percent of the mortar (%);  $P_a$  is the mortar aggregate passing rate (%), and  $P_a = 100\%$  in this equation;  $\gamma_a$  is the density of the asphalt ( $\text{g}/\text{cm}^3$ ); and  $VV_{m-r}$  is the air void content of the mortar with NMPS  $r$  (%). The final step is the calculation of the mortar voids, as shown in Equation (13); the top part of the fraction are the air voids in the mortar, and the bottom part of the fraction is the accumulated volume of voids, mortar aggregate and mortar asphalt. This equation is the calculation for a certain mortar NMPS and asphalt mixture type.

The air void content,  $VV_{m-r}$ , of a mortar with an NMPS is calculated as per Equation (13):

$$VV_{m-r} = \frac{VV \times v_{p-r}}{\left( VV \times v_{p-r} + \frac{P_{si-r}}{\gamma_{se-r}} + \frac{P_{a-r}}{\gamma_a} \right)} \times 100 \quad (13)$$

## 7. Equation Calculation Results and Analysis

### 7.1. Mortar Air Void Content Results

The expressway pavement consisted of an AC13 layer as the surface layer, an AC20 layer as the middle layer and an AC25 layer as the bottom layer, and the mixture's air void contents were 4%, 4.5% and 4.2%, like the commonly used mixture mentioned before. When designing the air void content of the mortar, we first determined the volume in this mortar with a certain mixture type, mixture air void content and mortar NMPS. The air void content of the mortar may larger or smaller than that of the mixture, because the total mortar volume consists of only some part of the whole mixture. For example, the calculation for the mortar with an NMPS of 2.36 mm, the void percent is 48.1%, 40.5% and 35.1%. The  $P_a$  values are 33.1%, 40.5% and 35.1%;  $\gamma_{se-r}$  are 2.74, 2.71 and 2.71  $\text{g}/\text{cm}^3$ ;  $P_{b-r}$  are 12.8%, 13.6% and 12.0%;  $\gamma_b$  is 1.03  $\text{g}/\text{cm}^3$ . For example, the air void content of the AC-13 mortar with an NMPS of 2.36 mm is:

$$VV_{AC-13-2.36} = \frac{4\% \times 48.1\%}{\left( 4\% \times 48.1\% + \frac{33.1}{2.74} + \frac{12.8}{1.03} \right)} \times 100 = 4.8 \text{ (\%)}$$

Using the same method to calculate the other mortars with different NMPS and mixture types, the results are shown in Figure 8. From Figure 8, the air void content of the AC-13 mortar is smaller than that of AC-20 and AC-25 with a certain NMPS. The air void content of the AC-13 mortar increases with an increasing NMPS.

With this calculation method, a more accurate air void content of the mortar can be obtained. From Figure 4, the air void content of a 0.6 mm mortar is approximately 1% and that of a 4.75 mm is approximately 8%. Different NMPS have a much smaller effect on the

air void content than mortar NMPS. With the increase in the mortar NMPS, the mortar air void content increases at the same time.

### 7.2. Results of the Sensitivity Analysis

Changing the air void content of the mixture could affect the mortar voids, and a commonly used asphalt aggregate ratio and air void content range were studied. The mortar void sensitivity analysis of the AC-13 mortar is shown in Figure 9.

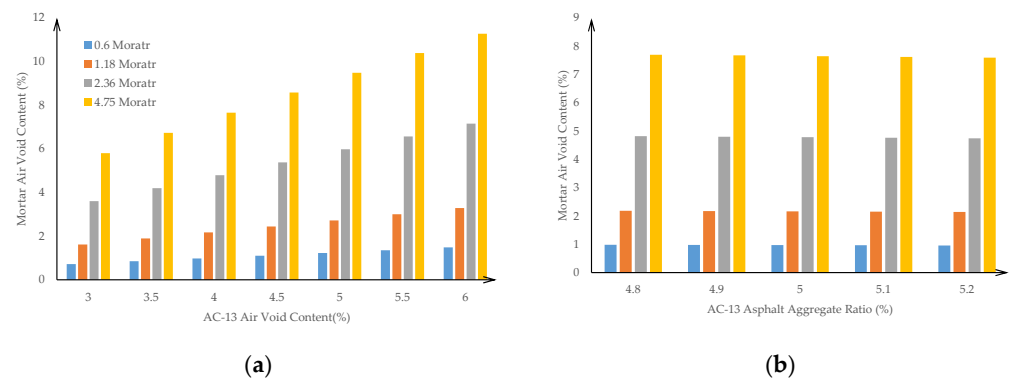


**Figure 9.** AC-13 mortar voids: (a) with different mixtures' air void content; (b) with different asphalt aggregate ratios.

AC-13 had a designed air void content of 4% and a designed asphalt aggregate ratio of 5%. Several changes were applied to the air voids and asphalt aggregate ratio. From Figure 9, it is revealed that the mortar with different NMPS had different sensitivities. For the mortar with a 0.6 mm NMPS, a 1% parameter value change in the air content or asphalt aggregate ratio in the corresponding asphalt mixture could lead to an approximately 0.1% change in the 0.6 mm mortar's air void content and a 1% change in the 4.75 mm mortar's air void content. The air void content of the mortar with a larger NMPS was more sensitive than that of a smaller NMPS. With same mortar NMPS, the air voids of the mixture were more sensitive to the mortar air voids than the asphalt aggregate ratio of the mixture. Because this result was calculated by the given design, the mortar air void content versus the different AC-13 air void contents had a significant linear correlation, and each coefficient of determination,  $R^2$ , was almost 1. These results were calculated by their scanned mixture samples; therefore, they had good correlation.

When changing the mixture air void content and asphalt aggregate, the mortar air void content of AC-20 and AC-25 are shown in Figures 8–10. The mortar air void content versus the different AC-20 and AC-25 air void contents had a significant linear correlation, and each coefficient of determination,  $R^2$ , was close to 1, similar to AC-13. The AC-13 slope absolute value of the mortar air void content versus the mixture air void content was bigger than that of AC-20, and AC-20's was bigger than AC-25's. This indicates that with the same mixture air void content as in AC-13, it would have a larger mortar air void content whether the mortar NMPS and the mixture with a lower NMPS had a higher mortar air void content sensitivity. The AC-13 slope absolute value of the mortar air void content versus the asphalt aggregate ratio was bigger than that of AC-20 and lower than that of AC-25, indicating that this slope absolute value did not have a clear rule with NMPS. The Figure 10 showed AC-20 mortar void content with different mixture's air void content and with different asphalt aggregate ratios. The Figure 11 showed AC-25 mortar void content with different mixture's air void content and with different asphalt aggregate ratios.

The sensitivity analysis of the mortar air void content was more sensitive with the air void content change and less sensitive with the common asphalt aggregate ratio change.

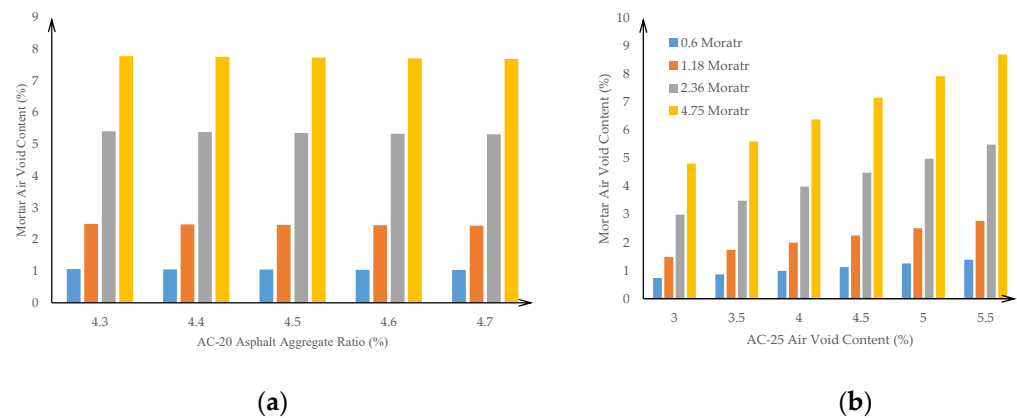


**Figure 10.** AC-20 mortar voids: (a) with different mixtures’ air void content; (b) with different asphalt aggregate ratios.

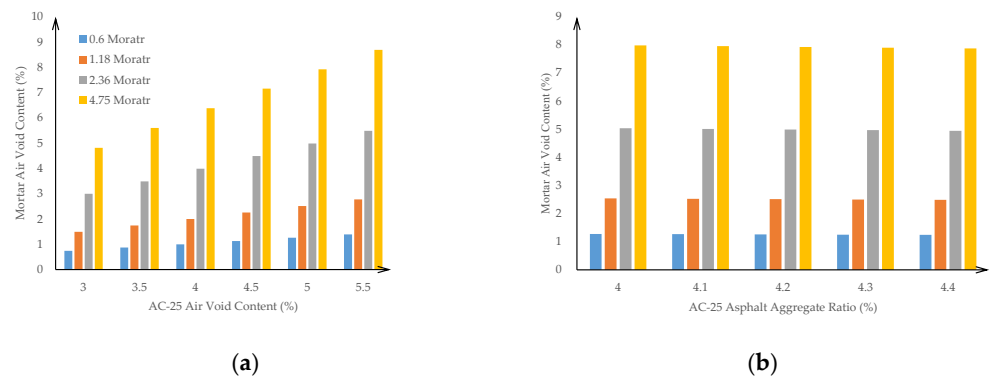


**Figure 11.** AC-25 mortar void: (a) with different mixtures’ air void content; (b) with different asphalt aggregate ratios.

### 8. Conclusions

1. Three commonly used asphalt mixture samples were scanned using industrial CT and the air void distribution and void passing rate of the samples were calculated. A new method for calculating a mortar’s designed air void content was created and used.
2. The mixture that had a small NMPS had a larger void percent, larger air void content and lower coarse aggregate percent for the mortar with a certain NMPS; for same gradation type, the mortar with the larger NMPS had a larger void percent and more air void content. The CT scanned air void content matched the tested air void content for the mixture samples.
3. The asphalt aggregate ratio had a lower impact on the mortar air void content, while the mixture air void content greatly affected the mortar air void content. The mortar with a 2.36 mm NMPS had an air void content that was closest to the mixture air void content; the mortar with an NMPS less than 2.36 mm had a lower air void content than that of the corresponding mixture; the mortar with a 4.75 mm NMPS had larger one than that of the corresponding mixture.
4. Both the mixture air void content and the asphalt aggregate ratio had a good linear correlation with the mortar air void of any NMPS.

**Author Contributions:** The authors confirm the contributions to the paper were as follows. Study conception and design: L.-H.S., F.-J.N. and J.-W.J.; test conduction: L.-H.S., Z.-L.Z. and Z.-Y.G.; data collection and analysis: L.-H.S. and Z.-L.Z.; draft manuscript preparation: L.-H.S.; review and editing: J.-W.J. All authors have read and agreed to the published version of the manuscript.

**Funding:** This research received no external funding.

**Institutional Review Board Statement:** Not applicable.

**Informed Consent Statement:** Not applicable.

**Data Availability Statement:** The data are included in this article.

**Conflicts of Interest:** The authors declare no conflict of interest.

## References

1. Li, R.; Leng, Z.; Yang, J.; Lu, G.; Huang, M.; Lan, J.; Zhang, H.; Bai, Y.; Dong, Z. Innovative Application of Waste Polyethylene Terephthalate (PET) Derived Additive as an Antistripping Agent for Asphalt Mixture: Experimental Investigation and Molecular Dynamics Simulation. *Fuel* **2021**, *300*, 121015. [\[CrossRef\]](#)
2. Khan, Z.H.; Tarefder, R.A.; Faisal, H.M. Multiscale Modeling of Asphalt Concrete and Validation through Instrumented Pavement Section. In *Transportation Research Record*; SAGE Publications Ltd: Thousand Oaks, CA, USA, 2021; Volume 2675, pp. 117–136.
3. Ding, Q.; Sun, Z.; Shen, F.; Huang, S. The Performance Analysis of Semi-Flexible Pavement by the Volume Parameter of Matrix Asphalt Mixture. *Adv. Mat. Res.* **2011**, *168–170*, 351–356. [\[CrossRef\]](#)
4. Kassem-Eyad, E.; Lytton, M.-R.; Chowdhury, A. Influence of Air Voids on Mechanical Properties of Asphalt Mixtures. *Road Mater. Pavement Des.* **2011**, *12*, 493–524. [\[CrossRef\]](#)
5. Gao, Y.; Cao, R. Research on the Design of AR-AC13S Mixtures. *J. Test Eval.* **2012**, *40*, 158. [\[CrossRef\]](#)
6. Zeiada, W.A.; Kaloush, K.E.; Underwood, B.S.; Mamlouk, M.E. Improved Method of Considering Air Void and Asphalt Content Changes on Long-Term Performance of Asphalt Concrete Pavements. *Int. J. Pavement Eng.* **2014**, *15*, 718–730. [\[CrossRef\]](#)
7. Aliha, M.R.M.; Amirdehi, H.R.F. Fracture Toughness Prediction Using Weibull Statistical Method for Asphalt Mixtures Containing Different Air Void Contents. *Fatigue Fract. Eng. Mater. Struct.* **2017**, *40*, 55–68. [\[CrossRef\]](#)
8. Yaylaci, M. The Investigation Crack Problem through Numerical Analysis. *Struct. Eng. Mech.* **2016**, *57*, 1143–1156. [\[CrossRef\]](#)
9. Yaylaci, M. Simulate of Edge and an Internal Crack Problem and Estimation of Stress Intensity Factor through Finite Element Method. *Adv. Nano Res.* **2022**, *12*, 405–414.
10. Ma, X.; Zhou, P.; Jiang, J.; Hu, X. High-Temperature Failure of Porous Asphalt Mixture under Wheel Loading Based on 2D Air Void Structure Analysis. *Constr. Build. Mater.* **2020**, *252*, 119051. [\[CrossRef\]](#)
11. Hu, J.; Liu, P.; Wang, D.; Oeser, M.; Tan, Y. Investigation on Fatigue Damage of Asphalt Mixture with Different Air-Voids Using Microstructural Analysis. *Constr. Build. Mater.* **2016**, *125*, 936–945. [\[CrossRef\]](#)
12. Guo, R.; Nian, T.; Zhou, F. Analysis of Factors That Influence Anti-Rutting Performance of Asphalt Pavement. *Constr. Build. Mater.* **2020**, *254*, 119237. [\[CrossRef\]](#)
13. Omairey, E.L.; Zhang, Y.; Soenen, H.; Carbonneau, X. Parametric Analysis and Field Validations of Oxidative Ageing in Asphalt Pavements Using Multiphysics Modelling Approaches. *Int. J. Pavement Eng.* **2022**, *20*, 1–24. [\[CrossRef\]](#)
14. Jiang, J.; Leng, Z.; Yang, B.; Lu, G.; Tan, Z.; Han, M.; Dong, Z. Penetration Mechanism of the Emulsion-Based Rejuvenator in Damaged Porous Asphalt Mixture: Microstructure Characterization and 3D Reconstruction. *Mater. Des.* **2022**, *221*, 111014. [\[CrossRef\]](#)
15. Wu, S.; Zhao, Z.; Xiao, Y.; Yi, M.; Chen, Z.; Li, M. Evaluation of Mechanical Properties and Aging Index of 10-Year Field Aged Asphalt Materials. *Constr. Build. Mater.* **2017**, *155*, 1158–1167. [\[CrossRef\]](#)
16. Khodadadi, M.; Khodaii, A.; Absi, J.; Tehrani, F.F.; Hajikarimi, P. Numerical and Analytical Length Scale Investigation on Viscoelastic Behavior of Bituminous Composites: Focusing on Mortar Scale. *Constr. Build. Mater.* **2022**, *350*, 128775. [\[CrossRef\]](#)
17. Ding, J.; Jiang, J.; Han, Y.; Ni, F.; Ma, X.; Li, Q. Rheology, Chemical Composition, and Microstructure of the Asphalt Binder in Fine Aggregate Matrix after Different Long-Term Laboratory Aging Procedures. *J. Mater. Civ. Eng.* **2022**, *34*, 04022014. [\[CrossRef\]](#)
18. Zhao, Z.; Jiang, J.; Ni, F.; Ma, X. 3D-Reconstruction and Characterization of the Pore Microstructure within the Asphalt FAM Using the X-Ray Micro-Computed Tomography. *Constr. Build. Mater.* **2021**, *272*, 121764. [\[CrossRef\]](#)
19. Underwood, B.S.; Kim, Y.R. Effect of Volumetric Factors on the Mechanical Behavior of Asphalt Fine Aggregate Matrix and the Relationship to Asphalt Mixture Properties. *Constr. Build. Mater.* **2013**, *49*, 672–681. [\[CrossRef\]](#)
20. Underwood, B.S.; Kim, Y.R. Microstructural Investigation of Asphalt Concrete for Performing Multiscale Experimental Studies. *Int. J. Pavement Eng.* **2013**, *14*, 498–516. [\[CrossRef\]](#)
21. Gardete, D.; Picado-Santos, L.; Capitão, S.; Luzia, R. Asphalt Mix Design: Discussion on the Bulk Specific Gravity Procedure Influence on the Results Obtained from Empirical, Volumetric, and Performance-Based Methods. *Constr. Build. Mater.* **2022**, *342*, 127870. [\[CrossRef\]](#)
22. Du, Z.; Yuan, J.; Zhou, Q.; Hettiarachchi, C.; Xiao, F. Laboratory Application of Imaging Technology on Pavement Material Analysis in Multiple Scales: A Review. *Constr. Build. Mater.* **2021**, *304*, 124619. [\[CrossRef\]](#)
23. Braz, D.; Lopes, R.T.; da Motta, L.M.G. Computed Tomography: An Evaluation of the Effect of Adding Polymer SBS to Asphaltic Mixtures Used in Paving. *Appl. Radiat. Isot.* **2000**, *53*, 725–729. [\[CrossRef\]](#) [\[PubMed\]](#)
24. Liu, J.; Wang, Y.; Wang, S.; Liu, Q.; Yu, B.; Wang, Q. Use of X-Ray Computed Tomography to Evaluate the Gradual Behaviour of Air Voids in Asphalt Mixtures during Permanent Deformation. *Int. J. Pavement Eng.* **2022**, *21*, 1–19. [\[CrossRef\]](#)
25. Hu, J.; Qian, Z.; Wang, D.; Oeser, M. Influence of Aggregate Particles on Mastic and Air-Voids in Asphalt Concrete. *Constr. Build. Mater.* **2015**, *93*, 1–9. [\[CrossRef\]](#)

26. Brahmajaree, N.; Kanitpong, K.; Sawangsuriya, A. Investigation on Internal Structural Properties of Asphalt Mixtures Subjected to Loading Using Image Analysis. *Int. J. Pavement Eng.* **2020**, *23*, 107–120. [[CrossRef](#)]
27. Xue, J.; Jiang, Y.; Zheng, Y.; Xiong, S. Optimization Design and Verification of SMA-13 Mixture Gradation Using Mortar Theory. *Constr. Build. Mater.* **2022**, *335*, 127478. [[CrossRef](#)]
28. Ministry of Transport of the People's Republic of China. *Technical Specification for Construction of Highway Asphalt Pavement JTG F40-2004*; China Communications Press: Beijing, China, 2001; pp. 12–14.
29. Gao, L.; Ni, F.; Luo, H.; Charmot, S. Characterization of Air Voids in Cold In-Place Recycling Mixtures Using X-Ray Computed Tomography. *Constr. Build. Mater.* **2015**, *84*, 429–436. [[CrossRef](#)]
30. Otsu, N. Threshold Selection method from gray-level histograms. *IEEE Trans Syst. Man. Cybern.* **1979**, *SMC-9*, 62–66. [[CrossRef](#)]
31. Liu, T.; Zhang, X.N.; Li, Z.; Chen, Z.Q. Research on the Homogeneity of Asphalt Pavement Quality Using X-Ray Computed Tomography (CT) and Fractal Theory. *Constr. Build. Mater.* **2014**, *68*, 587–598. [[CrossRef](#)]
32. Wu, W.; Li, Z.; Zhang, X.; Li, M. Evaluating RLWT Rutting Test of Asphalt Mixtures Based on Industrial Computerized Tomography. *Adv. Mater. Sci. Eng.* **2018**, *2018*, 1–8. [[CrossRef](#)]
33. Wollny, I.; Hartung, F.; Kaliske, M.; Liu, P.; Oeser, M.; Wang, D.; Falla, G.C.; Leischner, S.; Wellner, F. Coupling of Microstructural and Macrostructural Computational Approaches for Asphalt Pavements under Rolling Tire Load. *Comput.-Aided Civ. Infrastruct. Eng.* **2020**, *35*, 1178–1193. [[CrossRef](#)]
34. Du, C.; Liu, P.; Liu, Q.; Leischner, S.; Sun, Y.; Chen, J.; Oeser, M. Development of Locally Homogeneous Finite Element Model for Simulating the Mesoscale Structure of Asphalt Mixture. *Comput. Struct.* **2021**, *248*, 106517. [[CrossRef](#)]

**Disclaimer/Publisher's Note:** The statements, opinions and data contained in all publications are solely those of the individual author(s) and contributor(s) and not of MDPI and/or the editor(s). MDPI and/or the editor(s) disclaim responsibility for any injury to people or property resulting from any ideas, methods, instructions or products referred to in the content.